



Target effects during penetrator emplacement: heating, triboelectric charging, and mechanical disruption

Ralph D Lorenz *, Sarah E Shandera

Lunar and Planetary Lab, University of Arizona, Tucson, AZ 85721-0092, USA

Received 3 April 2001; received in revised form 18 July 2001; accepted 3 August 2001

Abstract

The violent emplacement of penetrators has effects on the target material which, while largely ignored to date, may be quite significant in the interpretation of scientific data returned from penetrators or may even cause system failures. These effects, for which we offer preliminary quantification, include heating of the target material, largely but not exclusively by frictional heating along the walls of the penetrator, the development of triboelectric charge, and the mechanical compaction, comminution and fracturing of the target material. The sparse and often difficult-to-obtain literature on these processes is summarized, and some unique preliminary experiments conducted in support of the NASA DS-2 Mars Microprobe mission are reported. We urge future spacecraft penetrator projects to pay attention to these interesting and important phenomena. © 2002 Elsevier Science Ltd. All rights reserved.

1. Introduction

Despite the lack of success in missions to date, the emplacement of penetrators into a planetary surface remains a significant technique that is likely to be necessary to enable a number of planetary missions (Kargl, et al., 2001; Kömle et al., 1997, 2001; Lorenz and Ball, 2001) such as the in-situ assessment of subsurface volatiles and thermal conditions or the establishment of seismological networks, on the Moon, Mercury, Mars, Io or elsewhere. Penetrator technology has been the purview of the military ballistics community for the last half century or so. Vast effort—both experimental and theoretical—has been devoted to understanding the parameters controlling the depth of penetration, and in ensuring the correct functioning of delivered equipment. While target effects such as comminution (the grinding of grains of target material) have been noted, they have only been of interest as influences on the penetration performance of the vehicle in question. Similarly, while electrostatic effects may have been present and noticed, prudent engineering practices such as grounding and shielding can largely eliminate their effects, and hence they have been studied little, if at all.

Many of these ‘incidental’ effects are of potential significance if the penetrator is intended to make delicate scientific measurements. For example, the thermal conductivity of the surface material may be estimated by monitoring the

cool-down of the penetrator after emplacement, with the assumption usually made that the surface material is uniform. However, the impact event itself has several effects which affect this measurement.

First, the impact deposits heat in the target which must be accounted for, and this heat may be distributed in an unexpected way. In addition to the frictional heating of a \sim mm thick film of target material, a volume heating may occur at much larger distances (cm) from the penetrator due to compaction of the target material. A principal planetary application of penetrators (e.g. Smrekar et al., 1999; Surkov et al., 1999) is to search for subsurface volatiles, notably water. Clearly, if the impact event causes significant heating, the volatiles will be mobilized. Conceivably this effect could be exploited to deliver the volatiles to a sensor, but more likely it means that great care must be exercised in acquiring the sample and interpreting data from it. It would be tragic indeed if a penetrator were to report an absence of water ice in a location abundant in it, except for a small dry cavity where the water was chased away by the penetrator’s energetic arrival.

Second, the target may be compacted (in the case of compressible and granular materials), fractured or comminuted (brittle materials), melted or all three. All these processes may affect the material’s physical properties such as its thermal conductivity.

Electromechanical phenomena are subtle, yet widespread, and indeed most accelerometers rely on some kind of electromechanical effect. Undesirable additional effects

* Corresponding author. Tel.: +1-520-621-5585; fax: +1-520-621-4933.
E-mail address: rlorenz@lpl.arizona.edu (R.D. Lorenz).

(i.e. ‘triboelectric noise’) often arise from compression of the insulator in cables during a dynamic event, or changes in cable capacitance as a cable unwinds, and these effects and other sources of electrical noise such as ground-loops are discussed in standard instrumentation texts and manuals (e.g. Serridge and Licht, 1987; Endeveco,¹ etc.). Of particular interest in this paper is the more classic triboelectric charging, where rubbing between two dissimilar materials separates charge and develops a potential between them, as in classroom demonstrations of static electricity. Such effects have been noticed, for example, on the wheel of the Sojourner rover on the Martian surface (Ferguson et al., 1999). The violence of penetrator emplacement gives ample opportunity to generate significant electrical charges, as we demonstrate.

The previous work into these phenomena is very sparse and somewhat scattered (and as regards triboelectric charging on penetrators, nonexistent, as far as this study could determine). The data at hand is not adequate to develop a full understanding of the phenomena and their effects. We present a summary of this previous work, and additionally present some new experimental results of our own. We recognize that even with these new data, our understanding is far from complete, and that this paper must serve only as a starting point for future investigations. However, since our survey of the literature has not revealed any comprehensive investigation of the effects we outline here, we believe this summary will be useful to other workers, and the detailed description of our tests may help them avoid some of the many difficulties in this field.

Our experiments were conducted in support of NASA’s DS-2 Mars Microprobe mission (Smrekar et al., 1999) which aimed to deploy 2 penetrators onto the surface of Mars. Among measurements which were to be made—the spacecraft were sadly lost on Mars in early December 1999—are a water detection experiment, impact accelerometry, and soil conductivity. Previous papers have described impact accelerometry experiments (Lorenz et al., 2000) and have demonstrated the usefulness of a breech pressure sensor for impact speed measurement in (Lorenz and Shandera, 2000).

2. Mechanical effects on target material

We discuss first the mechanical effects on the target material, since in a sense these are the starting point for the other phenomena. The mechanical effects can be considered in two parts: first the material must exert force on the projectile in order to slow it down—this upwards force must be due to pressure on the nose of the projectile, or friction along its sides, or both. Secondly, the target material must somehow accommodate the volume of the projectile itself

and possibly the tunnel left behind it. One aspect observed in previous studies in clay impacts is that the tunnel left by the penetrator is in fact slightly narrower than the penetrator itself, suggesting that some elastic deformation has occurred, with the wall of the tunnel ‘bouncing back’ after the passage of the penetrator. Anderson et al. (1996) discuss this effect in some detail. Where the target is consolidated, large-scale fracturing is a typical effect. Where the target is porous, compaction is a likely outcome. Kumano and Goldsmith (1982) describe an investigation, and Johnson (2001) has recently outlined a theoretical framework.

2.1. Previous work on comminution

Allen et al. (1957), in studies of the penetration of 1.30 cm diameter, 12.8 cm long, conical nosed projectiles into sand, noted an increase in the effective drag coefficient of their projectiles below a speed of 100 m/s. Due to this discontinuity, the authors propose that deceleration of the penetrator can be expressed in a form proportional to the square of the velocity at speeds above 100 m/s, whereas below this critical velocity v_c can be described by a term proportional to the square of the velocity plus an additional constant. The authors further conjecture that the critical velocity is associated with the speed of sound in sand, for which they cite theoretical and experimental values of 70 and 200 m/s, respectively. The angle of the nose cone was varied from 180° to about 10° . The authors found that for angles less than 90° the penetrator was unstable, and in the stable range the drag coefficient showed little dependence on the angle.

Allen et al. suggest collisions with sand particles for $v > v_c$ are inelastic, noting the presence of trails of finely-crushed sand where the projectile was above this speed, whereas for $0 < v < v_c$, the collisions are elastic and the grains are simply pushed aside. The kinematics of the impact are described by the decelerations $-dv/dt = \alpha v^2$ for $v > v_c$ and $-dv/dt = \beta v^2 + \gamma$ for $0 < v < v_c$, where α , β , γ are constants (note, however, that Allen et al. (1957) introduce some confusion in equating these parameters to a drag coefficient. Allen et al. do not state why, if v_c relates to crushing, it should be related to the speed of sound, rather than some strength-related parameter. They do, however, note that the sand starts to crush under loads of 100 bar or more.

Hakala (1965) fired several different flat-nosed penetrators (steel, tantalum, and aluminum with a steel cap) into Ottawa sand, using a microwave interferometry method to record the projectile’s position. Penetrators of two diameters (3.8 and 1.9 cm) and lengths ranging from 5.74 to 12.2 cm were used. Below a critical velocity (which he argues is related to the energy necessary to comminute the sand particles) Hakala models deceleration as proportional to velocity, while above the critical velocity it is related to the square of the velocity. The fact that Hakala’s v_c values are lower for larger projectiles suggests that something like a Reynolds

¹Endeveco Shock and Vibration Measurement Technology: An Applications-Oriented Short Course, Endeveco, San Juan Capistrano, CA, Part Number 29005.

number (i.e. with inertial forces divided by strength) is a more appropriate parameter for the onset of comminution than Mach number as implied by Allen et al. In principle, Hakala's interpretation is somewhat similar to that of Allen et al., although it seems to us that the formalism of a $v^2 + \text{constant}$ at low speeds, with the constant relating to strength, has a better (or at least more interpretable) physical basis than the 'viscous' (force proportional to velocity) relation of Hakala.

Hendrick and Gill (1977) find evidence that the zone of plastic deformation around a tool moving through soil decreases with increasing speed, and beyond the speed of plastic propagation in the soil (~ 10 m/s) compaction may not occur at all (although it is possible that the association with speed of propagation may be fortuitous, as for Allen et al., and in fact strength is the controlling parameter). The authors also note that the propagation velocity of stresses appears to decrease as the velocity of the tool increases. They suggest that phenomena at these speeds may effect the acceleration of a penetrator as it slows to the velocity of plastic propagation, possibly causing an otherwise unexpected increase in acceleration shortly before the penetrator comes to rest.

Mining industry studies have developed predictions of the velocity at which mineral grains can be crushed. Yashima et al. (1987) predict that $100\ \mu\text{m}$ particles quartz and feldspar would be expected to fracture at speeds of 50–70 m/s, while marble and limestone would fracture at 20–25 m/s, borosilicate particles at 225 m/s, and weak gypsum at 13 m/s. Fracture speeds are roughly proportional to the square root of particle diameter and so drop by about a factor of about 3 for particle sizes 10 times larger.

In a rather obscure report, A.P. French (1957) investigates the comminution of glass beads by a variety of small (0.22 in caliber) lead projectiles. The authors found that the crushed fraction of the bead volume swept by the projectile, when scaled by the diameter of the beads, was proportional to the square of the velocity. Fig. 1 shows their data on velocity and β/d , where β is the fraction of volume comminuted and d is the initial diameter of the glass beads. (Unsurprisingly, the crushing is a statistical phenomenon which increases steeply with increasing speed, rather than a 'threshold' process that only occurs above a certain speed.) A lower limiting velocity was introduced into the penetration equations and accounted for the same discontinuous effect noted by Allen.

2.2. Observations during EMRTC DS-2 tests

In support of the DS-2 probes flown to Mars, a series of tests were performed at the Energetic Materials Research and Test Center (EMRTC), operated at Socorro, New Mexico by New Mexico Tech. The penetration performance of DS-2 and impact accelerometer data recorded in these tests have been documented in an earlier paper (Lorenz et al., 2000). Briefly, a two-part penetrator comprising an aftbody 13 cm diameter, 10 cm long carrying a forebody 10 cm long, 4 cm

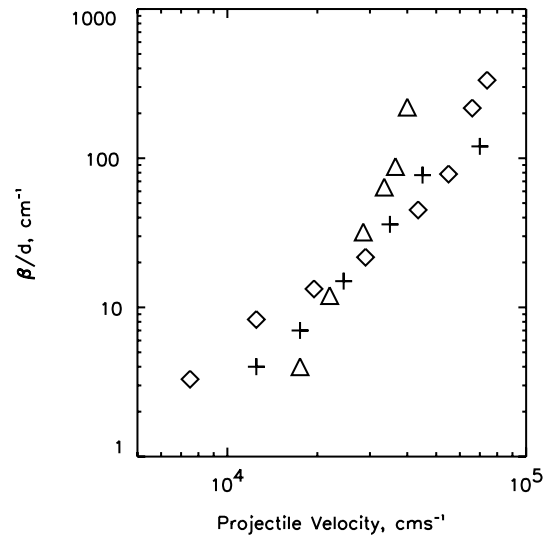


Fig. 1. Data from French showing the relationship between the fraction of material comminuted divided by the size of the target particles and the velocity of the penetrator. Crosses are 0.5 mm diameter glass spheres, diamonds 0.3 mm and triangles 0.1 mm.

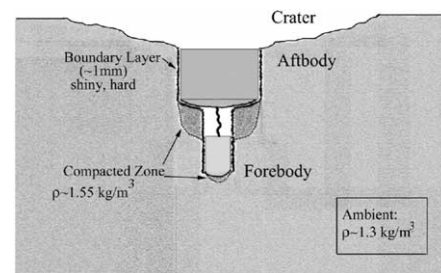


Fig. 2. Schematic of the compacted region around the DS-2 forebody during EMRTC DS-2 tests at 200 m/s impact speed. In some cases the forebody did not fully separate, and so was partly surrounded by the compacted zone ahead of the aftbody.

diameter projectile with a hemispherical nose was blasted into prepared soil targets at 200 m/s by a large airgun.

Although investigation of target effects was hampered by the need to download the accelerometer data within a few tens of minutes before the on-board battery expired, some observations were made during the excavation of the projectile. In particular, it was noted that the material adjacent to the projectile, and ahead of it, was compacted (see Fig. 2). In sand targets, however, this compacted zone was too fragile to remove intact (although it was present). Target material (and, inexplicably, foam from the sabot behind the aftbody) was compacted into any forward-facing cavity such as the weight-reduction holes bored into the face of the aftbody.

In clay targets, it was observed that clay surfaces on the tunnel that had been in contact with the moving forebody had a black, polished appearance. It could not be determined whether actual melting had occurred, but clearly this cannot be ruled out. This polished layer was too thin ($< \text{mm}$) and fragile to perform subsequent physical investigation.

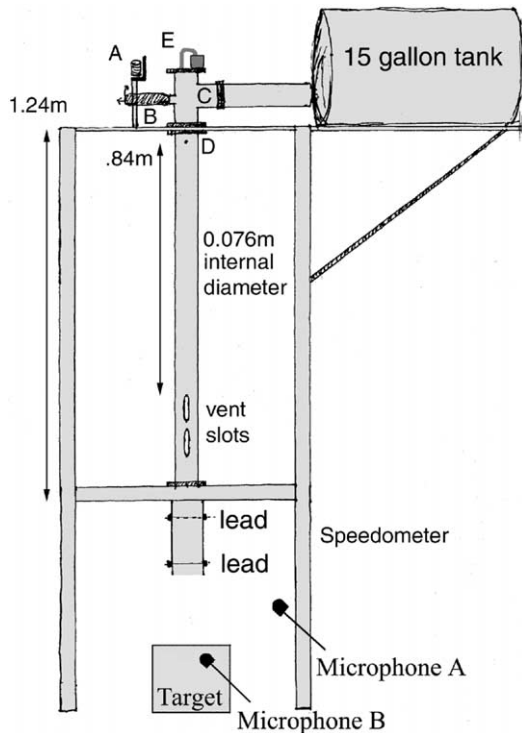


Fig. 3. Schematic drawing (to scale) of the airgun. Operation of the solenoid (A) raises the retaining arm (B) allowing the plunger valve in (C) to be pushed to the left and permitting air from the 60 l tank to flow into the breech. Pressure behind the projectile builds, recorded by the sensor (E) and causes the pin at (D) to fail. The projectile is accelerated down the barrel into the target.

The compacted zone below the aftbody, however, was large and strong enough to handle. Samples of both the compacted and uncompact clay were taken and subsequently weighed in air and oil to determine their density. The compacted material had a density of $1530 \pm 30 \text{ kg/m}^3$ while the surrounding material (not strictly 'uncompact', since the target material was tamped with a pneumatic hammer to obtain the desired target hardness—see Lorenz et al., 2000 for details) was 25% less dense.

2.3. Observations during UA DS-2 tests

A low-speed vertical airgun (Fig. 3) at the University of Arizona (UA) was constructed for investigations into the CRAF penetrator, and was used for subsequent experiments on coring penetrator samplers. The gun has also been used for impact accelerometry experiments on DS-2. The tests performed at UA have used a projectile similar to the forebody of the DS-2. The projectile (Fig. 4) is held in an aluminum sabot and accelerated to typically 40 m/s along a 2 m long airgun, driven by pressure released by a plunger valve from a large airtank.

Fig. 5 shows example data recorded during a shot: a wire-breaking speedometer using graphite pencil leads was used for initial shots, although it was later found

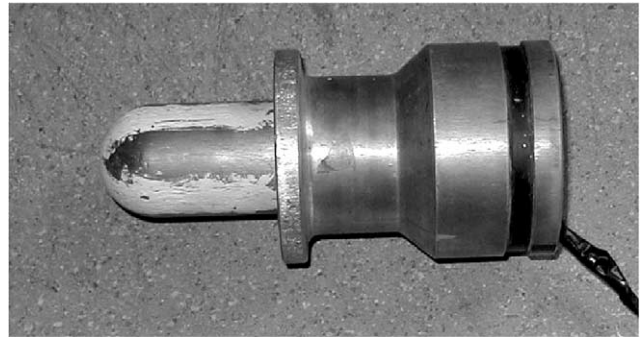


Fig. 4. Photograph of the projectile and sabot used in UA tests. The forebody has white witness paint to monitor abrasion. Narrow coax cable emerges at right from the (heavy) aluminum sabot.

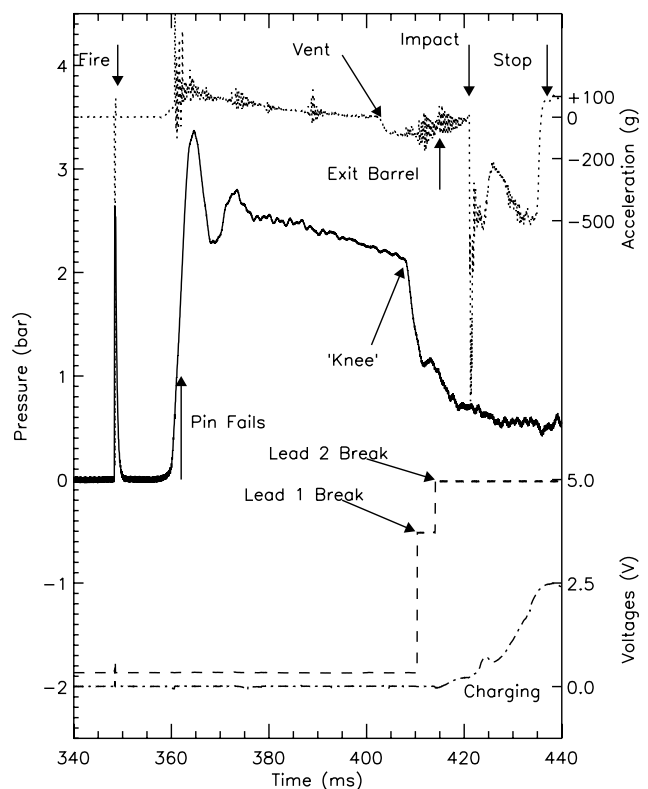


Fig. 5. Acceleration, velocity, charging, speedometer and pressure data obtained in a typical University of Arizona shot. The simultaneous acquisition of these different types of data is extremely helpful in interpreting the event. The time difference between the lead 1 and lead 2 signals, or the pressure data, are used to measure impact speed.

that speed could be satisfactorily measured using a breech pressure sensor. Fig. 6 shows some impact acceleration profiles into various targets not reported in Lorenz et al. (2000). In the DS-2 experiments it has been noted that the front part of the hemispherical nose usually has a packed deposit of finely ground material on it. Such a buildup presumably is peculiar to blunt-nosed projectiles which force some of the material to be crushed onto the nose.

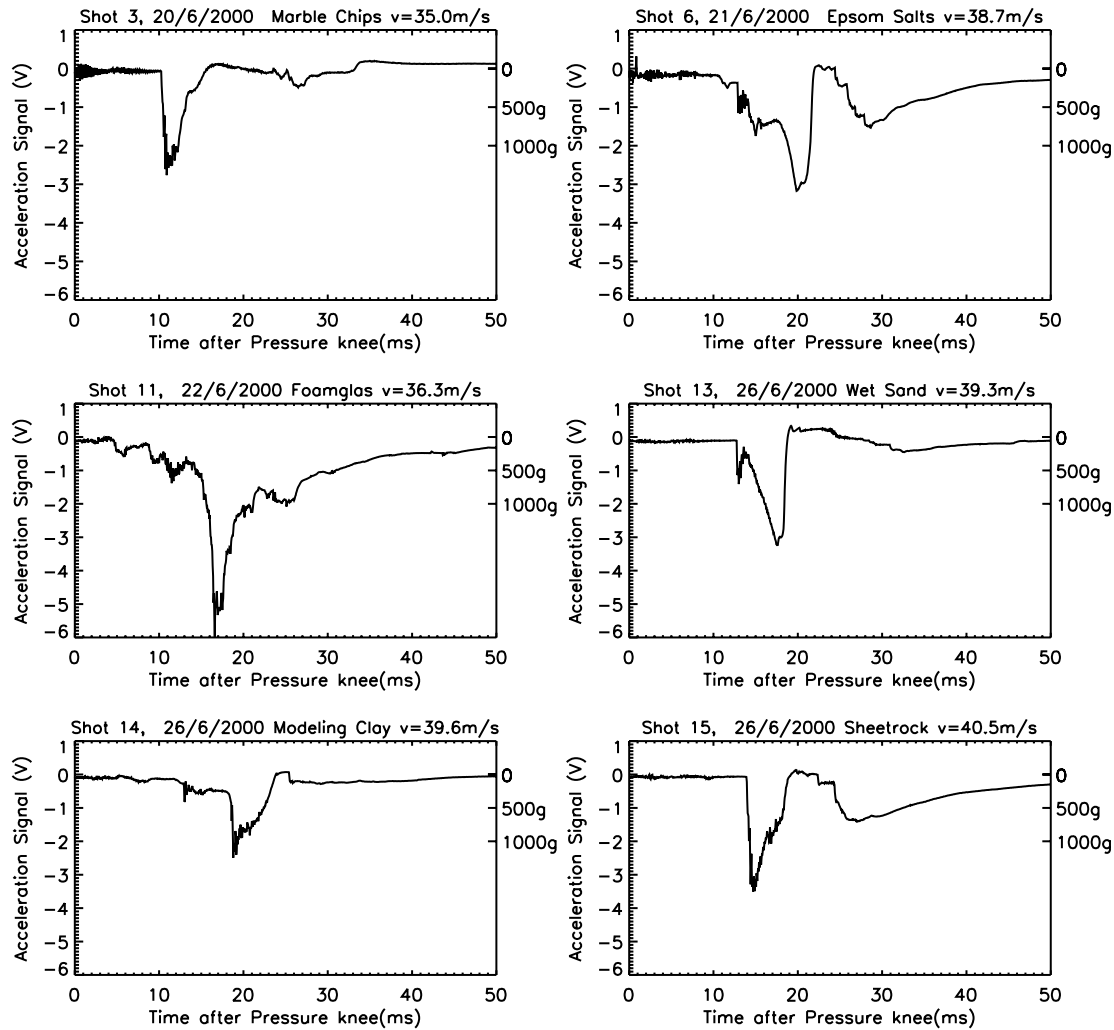


Fig. 6. Accelerometer records from impacts in various targets—note that the acceleration scale is only approximate and may be in error by a factor of several. The near-vertical onset of the impact signature seems to be associated particularly with the effective separation of the forebody from the sabot, usually in harder or denser targets.

UA impact tests into FOAMGLAS were found to be particularly good examples of comminution and compaction effects. FOAMGLAS is a glass foam used as industrial and household insulation (Pittsburgh Corning; density 128 kg/m^3 , compressive strength 700 kPa). When the material fails, it is crushed into a powder, but leaves a stark outline of the failure volume since the material just outside it retains its original shape: grooves of the order of mm wide could be seen in the FOAMGLAS left by imperfections in the penetrator shape. Shots were made with a hemispherical-nosed projectile into a stack of eight 7.6 cm-thick blocks. The penetrator typically came to rest midway in the fourth block ($\sim 26 \text{ cm}$ deep). The base of the tunnel formed in the material was a parabolic hole (Fig. 7): only part of this was filled by the hemispherical penetrator nose—the rest (approximately equal in volume to half the volume of the hemisphere) was filled with crushed FOAMGLAS powder.

Crater shape and the volume of crushed material pushed ahead of the nose were determined by sectioning blocks of cratered FOAMGLAS in halves or quarters. Fig. 8 shows one such cross-section. The crater is 60 mm deep and has an average radius of just over 20 mm (some variation is due to the act of cutting and tracing the edges, since the material is easily crushed). The hemispherical nose is superimposed to show how much of the crater is due to crushed material pushed ahead of the penetrator. The top (flat side) of the hemisphere sits about 22 mm down in the crater.

The shape of the impact crater is parabolic and flattened at the tip. The average parabolic fit for several cross-sections was used to calculate the volume of the crater minus the volume of the nose. Best results were obtained when the crater shape was clearly due to both the penetrator and crushed material. Occasionally, it was not clear if the penetrator nose had passed completely through a block of FOAMGLAS, or if the cone of material alone had broken through the bottom

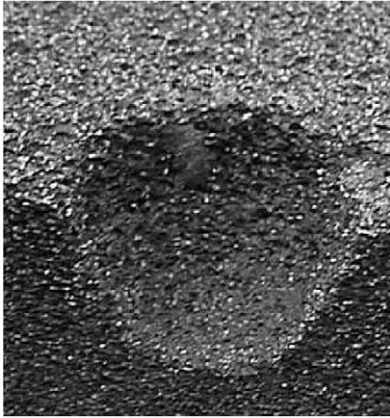


Fig. 7. Photograph of the parabolic hole formed and retained in FOAMGLAS by hemisphere-nosed projectile (40 mm dia.).

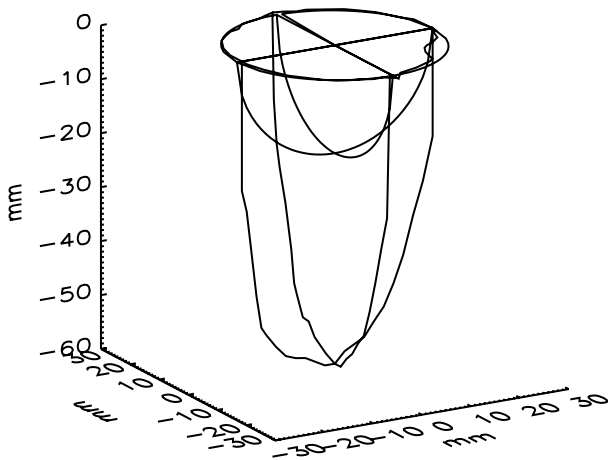


Fig. 8. Cross-section measurements of the parabolic hole formed by impacting FOAMGLAS. The hemisphere indicating the projectile nose is overlaid. The volume of crushed material filling the remainder of the crater was comparable to the volume of the nose itself.

of one block and into the next. In the latter case, a larger proportion of material was sprayed out between blocks and lost, making accurate volume measurements difficult. In general, the volume of the crushed material was approximately half the volume of the hemisphere.

Measurements made with a small shear vane in several blocks of FOAMGLAS gave a strength of 96 ± 10 kPa. The only strength value available from the product data sheets (Pittsburgh Corning, 2000) defines compressive strength as ‘the stress at which the main failure of the material occurs’ and reports a value of 689 kPa. We calculated an ‘effective strength’ for the material by dividing the kinetic energy of the penetrator at impact by the volume of the cavity formed by the forebody’s passage. These calculations give 970 ± 170 kPa—a good agreement with the published value. We note that bearing strength measurements with a small cone penetrometer at EMRTC also gave strength values a factor of 5 or so lower than those obtained by dividing impactor kinetic energy by the tunnel volume (Smrekar et al., 2001).

Thus small static penetrometers or shear strength gauges are likely to underpredict the effective strength for penetration by large projectiles. Although an inertial contribution to effective strength may be expected for dense targets (and is the principal distinction between static and dynamic penetrometry) since FOAMGLAS is such a low-density material, it is the length scale of structural strength that is likely to be the principal cause of the discrepancy here.

3. Impact heating

It is of course trivial to calculate the kinetic energy of a penetrator. Much less obvious is to understand how much of that impact energy is expended in deforming the target material (as in our calculation above), how much is radiated as seismic or acoustic waves, and how much is converted locally into heat. Given the empirical nature of most penetration investigations, this understanding has not been crucial to evaluating penetration performance. However, we argue here that such understanding may be important for both impact accelerometry measurements (whose interpretation is usually nonunique in terms of target properties) and for thermal measurements of subsurface thermal conductivity and geothermal heat flow.

In order to investigate the feasibility of using the rate of cooling of an initially-warm penetrator to measure thermal conductivity, a series of tests was made with a laboratory probe nearly identical to the DS-2 Mars Microprobes (Smrekar et al., 2001). The heated probe was drawn by a pulley system into a bed of glass beads (the whole assembly in a vacuum tank). Temperature data over the course of 24 h was recorded and modeled. Cooling was measured in both dust and sand grain sizes, and at several pressures. It was found that the thermal conductivity of the materials studied could be calculated to within about 10%, provided cooling information was available for more than the first several hours of cooling. However, the first few hours alone provided sufficient information to distinguish between uncemented dust and sand sized mediums, or to detect the presence of significant salt or ice. These results indicate that the method of determining thermal conductivity by penetrator cool down is in fact practical. Alternative methods of thermal properties determination requiring an active heat source (see, e.g. Seiferlin et al., 1996) do offer some advantages (the heating power can be controlled, experiments can be repeated and both warmup and cooldown curves can be studied) but generally sample a small volume and require additional hardware complexity. A penetrator cool-down approach averages the properties over a much larger volume (one that would require a prohibitive amount of energy to heat electrically) and thus is a valuable complement and/or backup to active techniques.

Smrekar et al. (2001) note that the initial cooling is steeper than would be expected—this may be an effect in part due to ‘forced convection’ during the emplacement

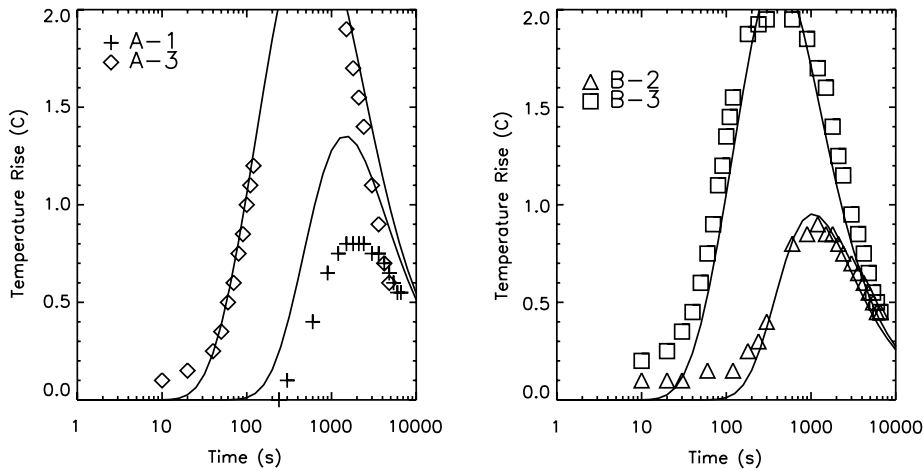


Fig. 9. Analytic fit (see equation in text) to data obtained by Reece in 1976 showing the temperature rise with time for thermistors located in the target soil. The ‘A’ thermistors were located 22 cm behind the nose of the projectile, A1 6.1 cm from it radially and A3 2.5 cm radially; the ‘B’ thermistors were 42 cm behind the nose, B-2 4.7 cm radially from the penetrator while B-3 was 2.2 cm away. The curve fits are for $\kappa = 2 \times 10^{-6} \text{ m}^2/\text{s}$ and $\Delta T = 10 \text{ K}$.

into the target—stirring of the material in closest contact with the penetrator body.

3.1. Previous work

Little work in general appears to have been performed (or at least documented) on the thermal effects of projectile impact. As noted in Backman and Goldsmith (1978), heating effects are typically ignored in models of projectile penetration because while the energy deposition increases as impact energy increases, the volume of material affected becomes smaller, so in general the effects may be neglected.

One study (Pitts and Canning, 1976) was performed in support of early Mars penetrator mission ideas. A large (28 kg) ogive-nosed penetrator was released from an aircraft, impacting the soil (loess) at 135–165 m/s, penetrating some 8 m. A thermistor array was inserted into the soil close to the buried projectile, and the outward-diffusing frictional heat pulse from the event was recorded. The heat deposition into the surrounding soil was calculated to be about 75 cal/cm (315 J/m), about 70% of the impact kinetic energy divided by the length of the hole. In-situ measurements of thermal conductivity at varying distances from the borehole are also made during recovery of the penetrator.

Reece (1976) reports temperature rises recorded by thermistors placed at various positions in the soil of a prepared silty sand target at Sandia Laboratories in Albuquerque. The penetrator was a 0.58 scale model Mars Penetrator (71.32 cm long, 5.18 cm in diameter, with an ogive nose and weighing 5.62 kg), which penetrated 1.97 m into the target. The temperature rises recorded by the thermistors are shown in Fig. 9.

Reece does not explore the implications of this data in any depth, but in fact an analytic approximation that allows a physical interpretation of the data is quite straightforward. The solid line fits shown in the figure are generated by the

equation for the evolution of the temperature perturbation (δT) with time (t) for a cylinder radius a , length b . The space inside the cylinder (i.e. $|x| < a$, $|y| < b$) has an initial temperature perturbation ΔT relative to the space outside the cylinder. The equation has the form (Carslaw and Jaeger, 2000, p. 56—note however, that I have changed to notation for clarity in this paper):

$$\delta T = \frac{1}{4} \Delta T \left\{ \operatorname{erf} \frac{a-x}{2(\kappa t)^{1/2}} + \operatorname{erf} \frac{a+x}{2(\kappa t)^{1/2}} \right\} \\ \times \left\{ \operatorname{erf} \frac{b-y}{2(\kappa t)^{1/2}} + \operatorname{erf} \frac{b+y}{2(\kappa t)^{1/2}} \right\}.$$

Here erf is the error function. Although the independent measurements of the thermal properties of the soil were not reported, the value of thermal diffusivity (κ , $2 \times 10^{-6} \text{ m}^2/\text{s}$) required to fit the data is quite reasonable for dense soils (see Fig. 9).

The energy deposited by the impactor is determined by the fit parameter ΔT , here 10 K. Clearly the analytic model above is slightly imperfect in that the thermal properties of the penetrator are not the same as those of the surrounding medium, and that the soil is not an infinite space. However, the approximation is certainly good to a factor of 2 or so. With that caveat aside, the temperature increment $\Delta T \sim 10 \text{ K}$ can be interpreted as an energy deposition of 50 kJ. Reece does not give the impact velocity, but estimating this from the penetration depth and other test conditions suggests close to 200 m/s: the heating pulse therefore accounts for some 25–50 % of the kinetic energy of the impactor.

Separately, the effects of the impact event on the material immediately adjacent to the penetrator were determined for two soil types. Results for sediment (silts and sands, simulating Martian plains) at McCook, Nebraska, and those for basalt (simulating Martian layered basalt flows) at Amboy, California are discussed in separate reports, (Blanchard

et al., 1977a, b). In both cases, detailed analysis of the mineral content of the soil surrounding the penetrator allowed the temperature and pressure changes induced by the penetrator's passage to be evaluated. Significant effects included soil contamination from the penetrator, migration of volatiles, and the formation of new minerals as those already present in the soil were crushed and melted. In basalt, these effects were found only within a 1 cm boundary of the penetrator, while in sediment the effects were limited to a 2 mm range.

Blanchard et al. (1976) estimate the skin of the penetrator reached a temperature between 1273 and 1673 K during impacts into sediment. The lower constraint comes from the presence of a thin glassy layer very close to the penetrator, which needed temperatures of at least 1273 K to form from the minerals present in clay. The upper bound is based on the absence of evidence for a liquid iron oxide phase, which would occur at 1673 K. A similar glassy layer formed during impacts in basalt required temperatures of about 1473 K, constraining the temperature of the penetrator's skin in that case to the temperature range 1473–1673 K.

Reece (1976) reports temperature sensitive paint placed on the 0.58 scale model Mars Penetrator and analysis of the metallurgical properties of the penetrator's nose following impact show the temperature of the nose reached 800–1000 K, while the surface of the cylindrical body 35 cm from the nose was between 333 and 380 K.

Finally, several experiments were performed in support of the DS-2 mission, although with penetrators rather larger than the eventual DS-2 flight configuration. Steel penetrators 5.5 cm in diameter (with ogive nose 3 CRH, 'caliber radius head') were launched vertically into arroyo sand, dry fluid plaster sand, and rock. After the projectile was shot into the target, three thermocouples were inserted and the temperature of the penetrator was measured. At the velocities obtained (62–110 m/s, using a firing pressure of 150 psi (11 bar)), and in an ambient temperature of about 283 K, the penetrator temperatures were recorded to be below 311 K (Lundgren, unpublished communication 1995). This latter measurement adds little to, but is at least consistent with, the energy deposition implied by Pitt and Canning's results.

3.2. DS-2 tests at EMRTC

As reported briefly in Smrekar et al. (2001) some exploratory thermal tests were also performed by us: these tests are described more fully here. A single Analog Devices LM335 temperature sensor (an inexpensive semiconductor device) was emplaced in the target material at a depth of 15–30 cm. The sensor was excited by a 1 mA current, and the voltage across it (equal to the absolute temperature in Kelvin divided by 100) was recorded by a laptop computer (running on its own battery) equipped with a Pico ADC-12

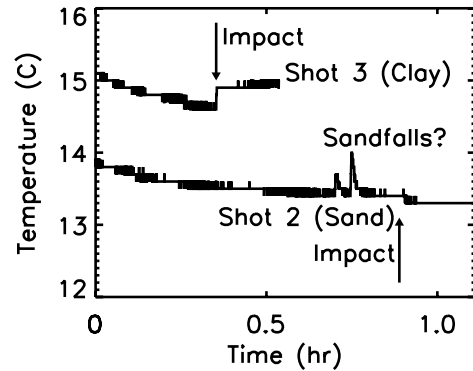


Fig. 10. Data from the buried LM335 temperature sensor during EMRTC tests. (a) Shot into sand. No impact event—the two recovering spikes are attributed to sand trickle. (b) Shot into clay—the step change occurs at the moment of impact.

16-bit analogue-to-digital converter. This unit plugs into the laptop's parallel port, making a convenient, self-contained unit.

The temperature sensor was emplaced in the target material by drilling a diagonal hole with a bent piece of stiff wire spun in a cordless drill. The location of the sensor was estimated to be within 5 cm of the impact point of the penetrator (the impact point on the surface was known from a laser beam that could be placed along the airgun boresight).

The datalogging computer was set running typically 20 min before firing (since the target area had to be cleared for safety reasons during the final gun pressurization and firing). The sampling rate chosen was 1 sample per second. The 16-bit accuracy and 5 V range of the converter implies a measurement precision of $5/16,384 = 0.3125$ mV or ~ 0.03 K.

On the first shot, into a fine quartz sand, the sensor was ejected from the target material, either by excavation in the impact itself, or by the scouring by the airstream (the muzzle of the gun was only ~ 2 m from the target and was not equipped with a muzzle brake).

In the second shot, the sensor was placed rather deeper (~ 30 cm), and was about 10 cm laterally from the impact point. The sensor remained in place, but did not detect any temperature perturbation. The data show a couple of anomalous spikes (Fig. 10), which are believed to be real temperature excursions, although spurious in the context of impact heating. The hole was not packed, and our interpretation of these temperature jumps is that warm sand (from near the surface) trickled down the hole, warming the sensor briefly before equilibrating with the cooler sand at depth. No thermal event that can be attributed to the impact event was detected over the 20 min or so following the shot (the projectile had to be excavated at this point in order to download the accelerometry data from its on-board datalogger).



Fig. 11. Photograph of the modified UA penetrator forebody with telephone cord cable and three LM335 sensors.

The third shot was into local New Mexico clay, and the hole was rather better packed. On this shot, an unexpected event occurred: the data show a +0.4 K step change in temperature at the moment of impact. Upon projectile excavation, it was found that a roughly cylindrical region of clay ahead of the aftbody had been compacted (Fig. 2), and the temperature sensor was embedded in this compacted zone.

During the process of target construction, the target strength (Lorenz et al., 2000) was measured with a drop-hammer penetrometer, and a static penetrometer. This latter instrument indicated that the cone bearing strength of the target (uncompacted clay) was 30–40 kg/cm², or 3–4 MPa. Thus the work done in compacting one cubic centimeter of material is (noting that the volume changes by 25% during compaction, see Section 2) $0.25 \times 10^{-2} \times 10^{-4} \times 4 \times 10^6$ or about 1 J.

Dividing this work done by a typical heat capacity of ~ 2000 J/kg/K gives a temperature increase of ~ 0.5 K during compaction, an encouraging agreement with that observed. Temperature measurements were attempted on the fourth shot, also into clay. On this test, the data abruptly fail at the moment of impact—the projectile sheared through the wires to the sensor.

3.3. UA tests

The accelerometry experiments used a small coaxial cable wound in the inside of the sabot to carry the accelerometer signals up to the breech of the airgun and out to an amplifier and datalogger. Since it was desired to record more than one temperature measurement on the penetrator, another cabling arrangement was tried. Three temperature sensors with a common ground require a fourth conductor cable. A coiled telephone handset cord, about 50 cm long (with a stretched length of 4 m) was tried, and found to work successfully. Indeed this arrangement sustained far less damage during each shot, and was much easier and quicker to set up than the coaxial cable. Three LM335 temperature sensors were embedded in epoxy resin along the length of a brass penetrator (see Fig. 11).

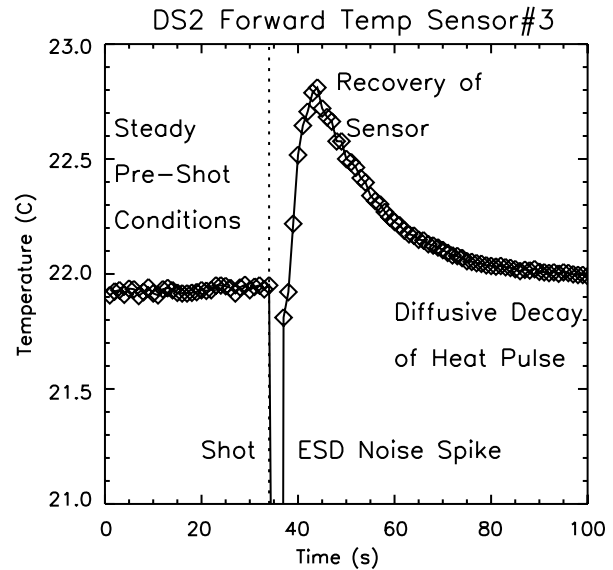


Fig. 12. Data from an LM335 temperature sensor just behind the nose of the forebody in UA test. Heat pulse and decay (muted by the thermal mass of the penetrator) are apparent, as is the anomalous behavior of the sensor for several seconds immediately after impact, attributed to triboelectric charging.

A definite temperature increase was noted at impact, typically 0.5 K. Since the target material was several degrees below the projectile temperature, the rise must be attributable to impact heating, and as shown in Fig. 12, the heat pulse decays somewhat. The forward temperature sensor showed the greatest rise, although usually the forebody did not completely separate, so the aft sensors were not in any case exposed to the sand target material.

It is seen that the temperature data rise to a peak about 50 s after the shot. This is to be expected in that the temperature sensors are behind about 3 mm of epoxy resin, which has the effect of low-pass filtering the thermal spike at impact. The time constant for this filter is approximately $\tau = (a/\kappa)^{0.5}$ with τ the delay, a the layer thickness (~ 4 mm, including the packaging of the sensor itself) and κ the thermal diffusivity ($\sim 10^{-6}$ m²/s), yielding $\tau = 63$ s, consistent with the delay observed.

It was noted that the measurements were corrupted for up to 30 s after the shot. It is conjectured that some kind of triboelectric discharge generated a potential on the sense wires that over-ranged the A-D converter. It was also observed that the epoxy had eroded somewhat, by about a millimeter after four tests.

Paint was applied to the forebody—it was observed (as expected) that the paint was eroded from the hemispherical nose, but was essentially untouched on the side of the forebody, indicating that frictional contact with the side of the forebody was minimal. Because of fear of damaging the data acquisition system with triboelectric voltage spikes, the separation difficulties, these tests were discontinued.

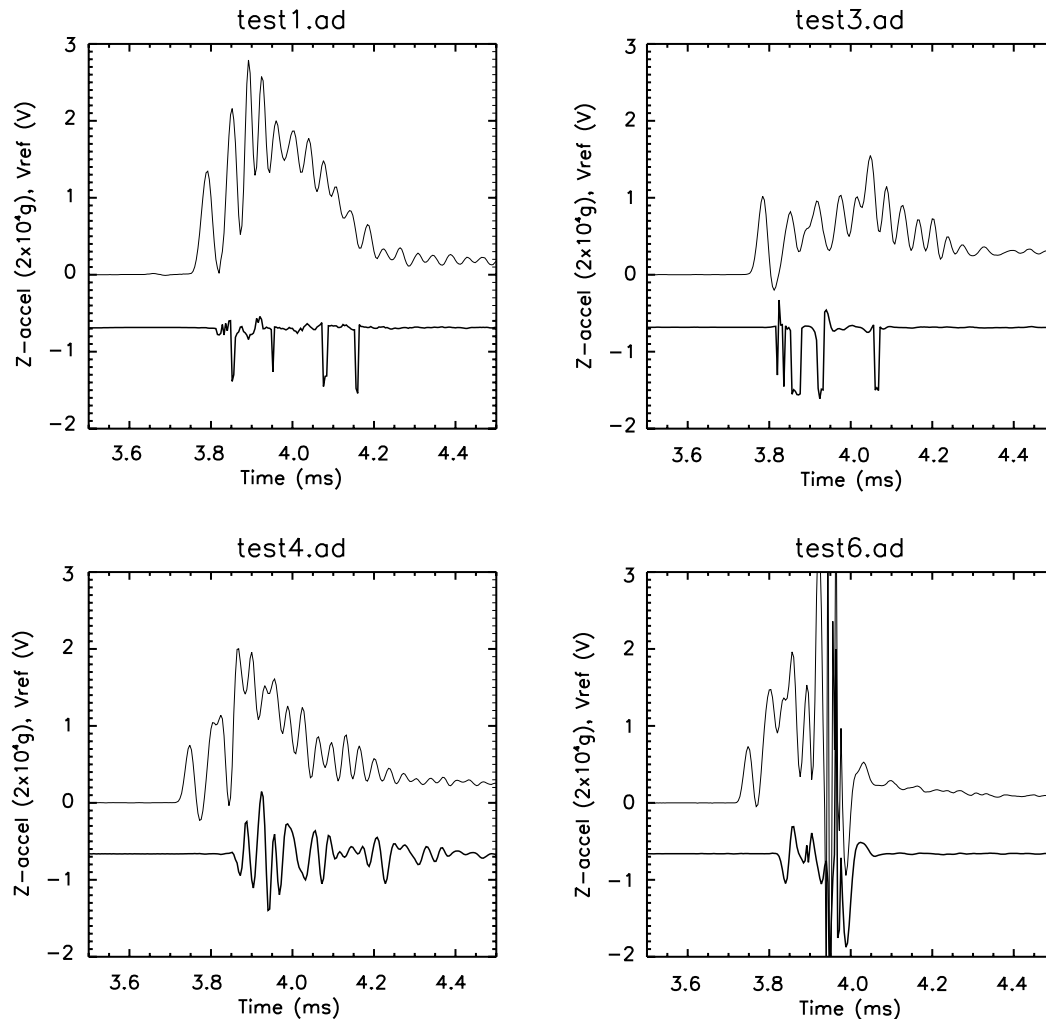


Fig. 13. Peaked Z-axis acceleration measurements (upper curves), and voltage (lower curve) signals across a bridge of $1\text{ k}\Omega$ resistors, recorded during 4 of 6 instrumented DS-2 shots at EMRTC (see Lorenz et al., 2000): voltages are displayed offset by 3 V for clarity. In shots 1 and 3 the voltage perturbations are more or less impulsive and unipolar, while in 4 a bipolar oscillating transient that correlates in amplitude with the deceleration is apparent (and may indicate acceleration-induced supply voltage fluctuations). In shot 6 a transient at 3.9 ms corrupts both the voltage and acceleration signals which are saturated.

3.4. Discussion and suggestions for future experiments

There is in our tests, and in the literature, evidence of heating effects which are detectable at 40 m/s, and very apparent at $>100\text{ m/s}$. It is likely that ogive-nose projectiles promote frictional heating compared with blunter shapes, but this has not been explicitly verified.

The relatively small temperature rise for low-speed impacts is difficult to measure reliably (given the harsh dynamic and electrostatic environment). Thermocouple gauges, might be more robust in this regard, and as they have small physical size and are clad in metal tubing, could be mounted on the skin and might be able to record the temperature rise during the impact itself with time constants of a few milliseconds. A combined investigation with a buried sensor array and penetrator-mounted impact heating measurements would be ideal.

4. Impact charging

Anomalies in temperature data during these latter tests were thought to be possibly due to triboelectric effects introducing charge transients onto the temperature sensor cabling—it had been noted that as very dry sand was poured into the target receptacle a crackling sound could be heard, presumably due to static discharge. Accordingly, a specific impact charging investigation was initiated since discharge events might be hazardous to penetrators with exposed conductors such as umbilicals. We found these experiments to be very challenging, so we record them in detail to guide the efforts of future workers.

It may be noted that the full-speed DS-2 impact tests conducted at EMRTC, New Mexico (Lorenz et al., 2000) recorded the voltage on a pure resistor bridge, as well as on bridges including the piezoresistive accelerometer elements. Transients on this resistor channel (Fig. 13) would

presumably be due to instantaneous change in the resistance of bridge elements, to drops in excitation voltage of the bridge, or to voltages applied to the sensing or excitation conductors in the umbilical. Some changes appear as spikes, suggesting supply voltage spikes due to instantaneous open-circuits or discharge onto the umbilical, while others are strongly correlated with the acceleration signal.

For tests at UA, a high-impedance JFET op-amp chip was used as an electrometer: any charge induced on the input terminal (connected to the body of the penetrator) would be shared between the capacitance of the penetrator itself (which is very low) and the capacitor connected across the input terminals of the op-amp. Using a LF356 chip (an inexpensive and readily-available device) with a ceramic 47 nF capacitor and without taking any particular precautions such as circuit board cleaning or low-loss component selection, the e-folding time for charge decay was over 100 s.

In the course of the latest series of UA experiments we have attempted to record evidence of charging on impacts into dry sand, damp sand, clay, FOAMGLAS, rock salt and MgSO_4 . In an attempt to most accurately (and consistently!) determine the magnitude and sign of charging, our method of measurement evolved throughout the experiment. Fig. 14 shows the three circuits used; in all cases the charge signal was recorded by the laptop data acquisition program. The method used for each shot is noted in Table 1, as is the specific circuit element included at the position marked X in the figure. Impacts into FOAMGLAS, dry sand and rock salt produced charge, but no charge was observed on impacts into damp sand or clay.

In Fig. 15, the voltage on the charge channel, can be seen to rise by about 2.5 V during the impact event (it subsequently decreased, presumably to the pickup of stray charge that was suppressed by grounding of the projectile in the barrel before and during firing) The increase is obviously associated with the impact event. The charge deposited on the capacitor corresponds to $2.5 \text{ V} \times 47 \text{ nF}$ or 120 nC. This corresponds to a charging current of some 6 μA .

Without the capacitor into which to dump this charge, the 120 nC charge deposited could lead to potentials of many hundreds or thousands of volts, since the capacitance of the penetrator and cable alone were only some tens or hundreds of picoFarads: these high voltages could have deleterious effects on sensitive electronics.

Fig. 16 shows that the impact charging current with this arrangement (circuit A, using the screen of the accelerometer cable as a charge sensor cable) seems closely related to the force on the penetrator as indicated by the accelerometer signal. That particular association may be due to some kind of coupling between the piezoelectric accelerometer and the charge measurement but deserves further investigation. To at least partially eliminate that possibility we measured charging using a simple wire, with no accelerometer installed on the projectile. Charging was still observed.

We observed no charging on impacts into electrically conductive targets (moist clay and wet sand). We did not

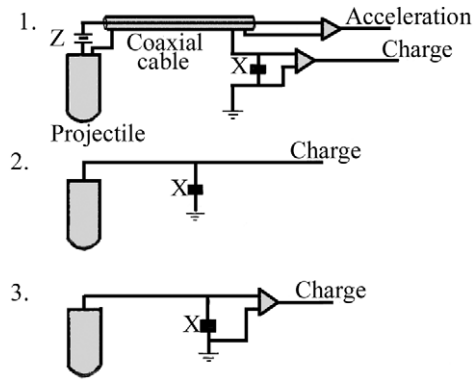


Fig. 14. Schematic of the three circuits used in UA triboelectric charging tests. The value of component X for each shot is noted in Table 1.

successfully observe any other consistent dependence of impact charging on target material type (for example, following some simple sand-pouring experiments, we hoped to detect charging of opposite sign on impacts into epsom salts and quartz respectively), although it was apparent that charge was more consistently generated when the forebody travelled further in the target. We confirmed that the charge generation was unrelated to the teflon liner between the penetrator forebody and the sabot by replacing the liner with one made from aluminum foil.

To step away from the spurious charging current effects that would cause the 'electrometer' type sensor to go into saturation after a few seconds unless grounded, we tried measuring the voltage across a resistor wired between the projectile and ground. Although partially successful, this approach was more sensitive to electrical noise from equipment in the nearby machine shops, and improper selection of the resistor led to over-ranging of the analog-to-digital converter on our datalogging computer. A fairly successful arrangement used a capacitor and resistor in parallel—the resistor giving a time constant of a microsecond or so eliminated any spurious background currents, while the capacitor limited the potential to which the electronics were exposed. Test 32 (Fig. 16) measured this way indicates a charging current of 3 mA for about 1 ms—again a few μC of charge. The short duration of the charging event is interesting and not yet explained. The penetrator generally acquired a positive charge.

4.1. Discussion

Blowing sand can acquire positive charges of 60 $\mu\text{C}/\text{kg}$ (Schmidt et al., 1998) while sand poured through a metal funnel generally acquires a negative charge (hence the funnel, like the penetrator in our experiments, became positively charged); blowing snow tends to have a negative charge. Electrostatic separation of minerals exploits that fact that quartz sand grains typically acquire a significantly different charge from that on other minerals such as calcite, dolomite and apatite, although the sign and magnitude of

Table 1
Results from the latest series of UA tests

Shot	Date	Target	Firing pressure (psi)	Penetration depth (cm)	Speed from lead break (m/s)	Speed from pressure sensor (m/s)	Test description	Results	Kinetic energy (J)	Vol. displaced (m ³)	Calculated strength (k Pa)
1	6/20/00	sand	40				Acceleration, pressure, speedometer and charge (1)	No data acquired (operator error)			
2	6/20/00	slightly packed sand	40		39.5	36.9	Acceleration, pressure, speedometer and charge (1)	Good data on all channels. ~ 92 nC charge			
3	6/20/00	15 cm layer of marble chips over sand	35	0–5	35.9	33.6	Acceleration, pressure, speedometer and charge (1)	Good data on all channels. ~ 92 nC charge			
4	6/21/00	epsom salts (MgSO ₄)	40				Acceleration, pressure, speedometer and charge (1)	No data acquired (operator error)			
5	6/21/00	epsom salts (MgSO ₄)	40			36.2	Acceleration, pressure, speedometer and charge (1)	Accelerometer cable broke during firing			
6	6/21/00	epsom salts (MgSO ₄)	40		38.7	37.0	Acceleration, pressure, speedometer and charge (1)				
7	6/21/00	sand	40				Acceleration, pressure, speedometer and charge (1)	No data acquired (operator error)			
8	6/21/00	8 3 in blocks of foamglass	40	26.2	42.0	37.9	Acceleration, pressure, speedometer and charge (1)	Data acquired, accelerometer over-ranged	430	0.00033	1306
9	6/21/00	8 3 in blocks of foamglass	55	47.0	47.1	41.9	Acceleration, pressure, speedometer and charge (1)	Good data, but accelerometer uncalibrated	526	0.00059	891
10	6/22/00	8 3 in blocks of foamglass	35	18.1			Acceleration, pressure, speedometer and charge (1)	Uncommanded firing prevented full analysis			
11	6/22/00	8 3 in blocks of foamglass	40	26.0	36.3	33.7	Acceleration, pressure, speedometer and charge (1)	Good data, but accelerometer uncalibrated	341	0.00033	1041
12	6/22/00	wet sand	40		39.6	35.8	Acceleration, pressure, speedometer and charge (1)	Cable broke during firing			
13	6/25/00	wet sand	40	12.0	39.3	35.8	Acceleration, pressure, speedometer and charge (1)	Good data. No charging measured	385	0.00015	2553

14	6/25/00	clay	40	42.4	39.6	35.9	Acceleration, pressure, speedometer and charge (1)	Good data. No charging measured. Remarkable effects in clay (plastic deformation)	386	0.00053	724
15	6/25/00	sheet rock, supported by 3 3 in blocks of foamglass	40	4.3	40.5	36.3	Acceleration, pressure, speedometer and charge (1)		395	0.00005	7311
16	6/28/00	8 3 in blocks of foamglass	40	30.5	36.7	33.7	Pressure, speedometer and charge (1). An ogeive nosed projectile was used	Wire break prevented full analysis			
17	6/28/00	8 3 in blocks of foamglass	40	30.5	34.8		Pressure, speedometer and charge (1). An ogeive nosed projectile was used	Data corrupted by AC noise?	340	0.00038	887
18	10/13/00	sand	40			36.0	Acceleration, pressure, speedometer and charge (1, $X = 1 \text{ k}\Omega$)	Data corrupted by AC noise?			
19	10/13/00	sand	55			42.2	Acceleration, pressure, speedometer and charge (1, $X = 1 \text{ k}\Omega$)	Data corrupted by AC noise?			
20	10/16/00	sand	40			39.1	Pressure, charge (2, $X = 500 \Omega$), microphones A and B.				
21	10/16/00	sand	40	6.4		39.0	Pressure, charge (2, $X = 500 \Omega$), microphones A and B, A amplified		455	0.00008	5704
22	10/16/00	8 3 in blocks of foamglass	40	27.9		36.3	Acceleration, pressure, charge (2, $X = 500 \Omega$), microphone A amplified.	Good seismic signal on B	394	0.00035	1123
23	12/11/00	sand	40				Pressure, charge (3, $X = 150 \Omega$), microphone A amplified, bucket charge	Good seismic signal on B			
24	12/11/00	sand	40			36.7	Pressure, charge (3, $X = 150 \Omega$), microphone A amplified, bucket charge (grounded)				
25	12/11/00	sand	40			38.4	Pressure, charge (3, $X = 150 \Omega$), microphone A amplified, bucket charge				

Table 1 *Continued.*

Shot	Date	Target	Firing pressure (psi)	Penetration depth (cm)	Speed from lead break (m/s)	Speed from pressure sensor (m/s)	Test description	Results	Kinetic energy (J)	Vol. displaced (m ³)	Calculated strength (k Pa)
26	12/11/00	sand	40			37.0	Pressure, charge (3, $X = 150 \Omega$), microphone A amplified, bucket charge				
27	12/11/00	extra coarse salt	40			36.7	Pressure, charge (3, $X = 150 \Omega$), microphone A amplified, bucket charge (grounded)				
28	12/11/00	extra coarse salt	40			36.9	Pressure, charge (3, $X = 150 \Omega$), microphone A amplified, bucket charge				
29	12/11/00	sand	40			37.4	Pressure, charge (3, $X = 150 \Omega$), microphone A amplified, bucket charge.				
30	12/20/00	sand	40			37.2	Pressure, charge (3, $X = 150 \Omega$), microphone A, bucket charge. teflon liner replaced with foil	Data corrupted by noise			
31	12/20/00	sand	58	7.6		40.9	Pressure, charge (3, $X = 150 \Omega$), microphone A amplified, bucket charge. Foil				

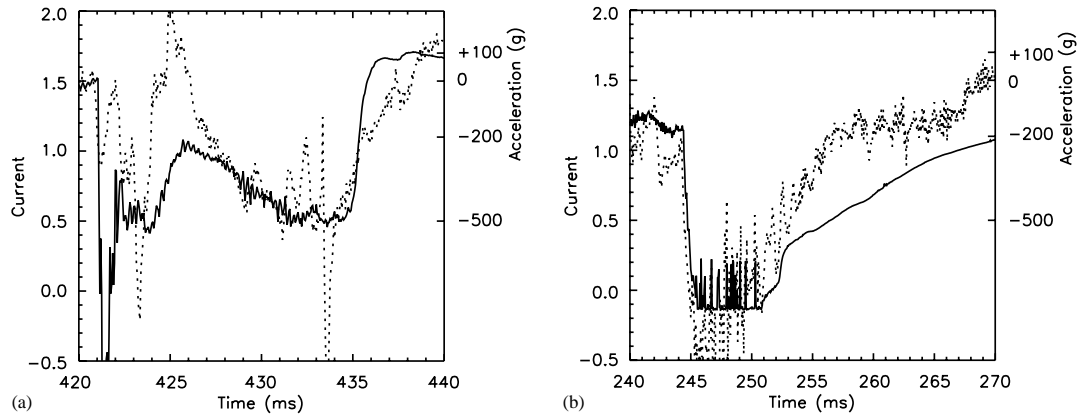


Fig. 15. Derivative (dotted line) of the charge sensor channel (i.e. proportional to the triboelectric charge current, in arbitrary units) superimposed on the accelerometer measurements (solid line). The agreement is compelling, suggesting (unless these signals are some kind of crosstalk from the accelerometer) that the charging mechanism and the forces retarding the projectile are closely related. (a) Shot into sand. (b) Shot into FOAMGLAS—the accelerometer measurement channel saturated on this shot.

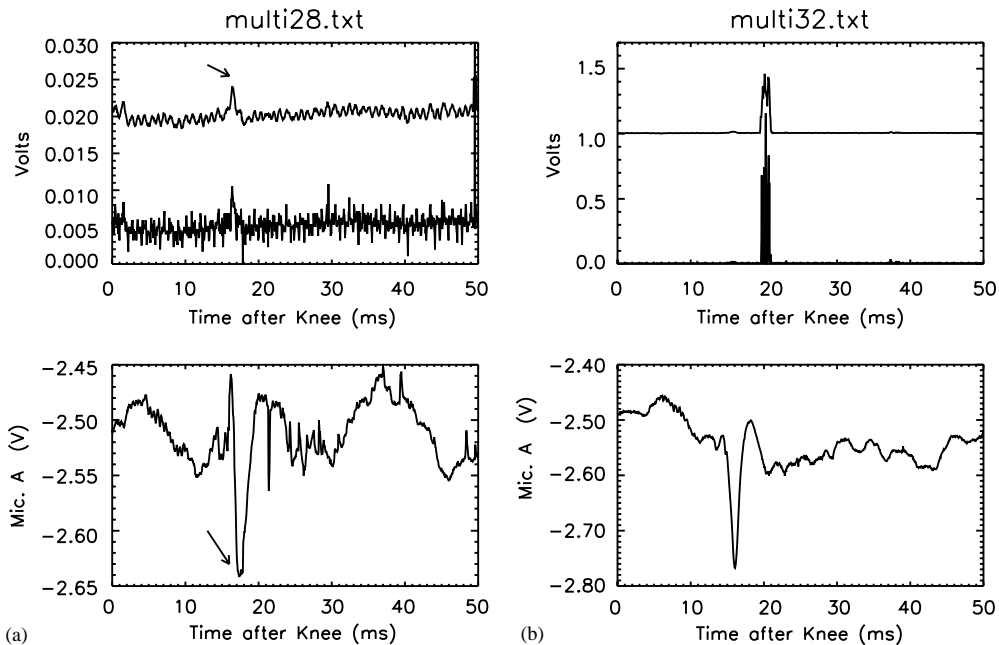


Fig. 16. Signals from the charge sensor (upper box, with smoothed version of signal displaced upwards for clarity) and microphone A (lower box). It is not clear whether the strong negative peak in the microphone signal is a pressure pulse related to the projectile leaving the gun barrel or to the impact itself. In the two tests shown here (28 and 31, respectively) there is about a factor of 100 difference in deposited charge.

the charge can depend on surface treatments, see also Fassio et al. (1982). NaCl, KCl, and KBr have been reported to acquire positive charges similar in magnitude to that of quartz. Interestingly, Jayaratne (1991) reports that adding a small amount of NaCl to ice reverses the sign of the charge acquired by ice in contact with sand—pure water ice charges positively, but in a 10^{-3} mol/l salt solution, the charge is negative.

Scattered reports note that many parameters of the materials and ambient conditions significantly affect the sign and magnitude of charge acquired by impacts. Bailey (1993)

compiles results on the triboelectric charging of powders and solids. Findings of note include that the sign of charge acquired by polymers contacting a metal surface can reverse above a certain temperature (~ 423 K), and that powders can acquire charge of both signs, varying with relative humidity. Considering the high temperatures and migration of volatiles associated with penetrator emplacement, both effects could contribute to wide variations in charging phenomena. Additional factors that have been noted include the size of particles affecting the sign of charging (Bailey, 1993; Schmidt et al., 1998) and, at least for

sand-ice charging, temperature affecting the magnitude of charging (Jayaratne, 1991).

Thus in summary, triboelectric charging appears to be extremely sensitive to target composition and environmental effects. The somewhat inconsistent results we have obtained are therefore to be expected from the combination of this sensitivity, the violence of the impact event and the difficulty of making these measurements.

Our principal conclusion, that charging events can and do occur during penetrator impact, appears robust, however. Whether charging measurements can be used to infer anything about the physical or chemical properties of the target (other than that it is wet) remains to be seen with more controlled experiments.

5. Seismoacoustic measurements

Purely as an experiment, we mounted a small piezoelectric microphone (A in Fig. 3) near the muzzle of the air-gun. A separate sensor (B), a piezoelectric-coated metal disk (usually used as a loudspeaker on clocks etc.) was attached with adhesive tape to the wall of the steel bucket used to hold the target material.

These sensors did record signals associated with the impact (Figs. 16 and 17) but their interpretation appears difficult. Since the duration of the excitation event is comparable with the transit time of acoustic signals to the sensors, it is difficult to relate any features to particular parts of the penetration process.

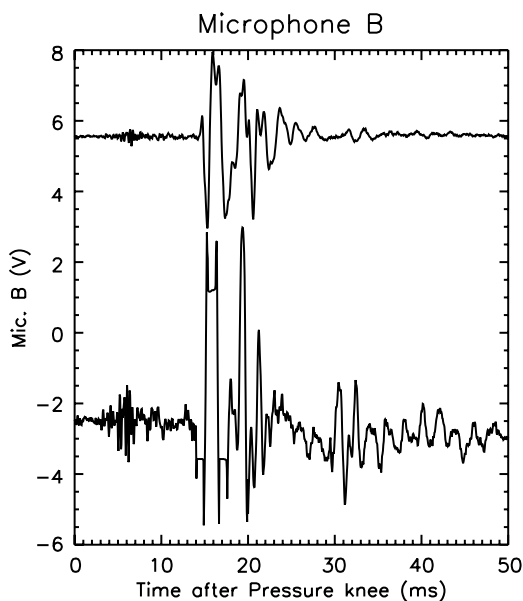


Fig. 17. ‘Seismic’ signals of impact, recorded with a piezoelectric disk microphone taped to the target bucket (shot 22 lower curve, shot 23 upper curve).

We think it useful to show these data as a ‘proof of concept’. A more concerted measurement effort, with arrays of sensors that can be correlated to isolate source regions like the contact site, should be able to provide further insight into the penetration process.

Properly-calibrated microphones or geophones, measuring target-coupled (rather than aerially-coupled) signals should be able to measure the seismic energy radiated from the target, see Fig. 17. This will be useful in understanding the energy partitioning during the impact event, and in assessing the usefulness of penetrator impact as a source of excitation for seismometers on the surface of a planetary body (see also Kochan et al., 2000).

6. Conclusions

A survey of the literature, and our own experiments, indicate that severe comminution of the target material can occur. The speed at which this occurs may be indicative of the material strength. We have observed the sharp plug nose of crushed target material formed by the passage of a blunt-nosed projectile.

The generation of a heat pulse itself occurs in milliseconds during the impact itself; the subsequent evolution has timescales of seconds to days. Both of these aspects may be in some sense diagnostic of the target thermomechanical properties. An understanding of the heating and compaction effects—*both of which probably depend on projectile nose shape*—is important in the interpretation of subsequent thermal evolution of the penetrator to deduce target thermal properties.

Triboelectric charging has been observed to occur during impact. Although obvious when articulated, the deposition of charge on objects moving at high speeds through sand does not appear to have been studied before. Although the potential to exploit charging experimentally to deduce target properties, seems uncertain, the phenomenon is important in that it may cause electrical problems for penetrators or their instrumentation.

These measurements are challenging, but offer continuing surprises and at least the promise of understanding the impact process better. We hope other workers are motivated to study their target materials in more detail and record impact data other than simple accelerometry.

Acknowledgements

We thank Jeff Moersch, now of the University of Tennessee, Andy Stone and Ron Morgan of JPL, and Kent Harvey and the staff at EMRTC for assistance with the tests in New Mexico. Bill Verts, Mike Williams and Brett Lawrie of the LPL Machine Shop are thanked for their patient assistance with the tests at UA. This work was supported by NASA via the New Millennium DS-2 project. SE Shandera was supported during part of this work by a grant from

the Arizona Space Grant Consortium. Karsten Seiferlin and Norbert Kömle are thanked for their careful and constructive reviews.

References

- Allen, W.A., Mayfield, E.B., Morrison, H.L., 1957. Dynamics of a projectile penetrating sand. *J. Appl. Phys.* 28 (3), 370–376.
- Anderson, W.W., Ahrens, T.J., Gibson, A., Scott, R., Suzuki, K., 1996. Emplacement of penetrators into planetary surfaces. *J. Geophys. Res.* 101 (E9), 21137–21149.
- Backman, M.E., Goldsmith, W., 1978. The mechanics of penetration of projectiles into targets. *Int. J. Eng. Sci.* 16, 1–99.
- Bailey, A.G., 1993. Charging of solids and powders. *J. Electrostatics* 30, 167–180.
- Blanchard, M., Oberbeck, V.R., Bunch, T., Reynolds, R.T., Canning, T., Jackson, R.W., 1976. FY 1976 Progress Report on a Feasibility Study Evaluating the Use of Surface Penetrators for Planetary Exploration, November 1976, NASA Technical Memorandum TM X-73,181.
- Blanchard, M., Bunch, T., Davis, A., Shade, H., Erlichman, J., Polkowski, G., 1977a. Results of analyses performed on basalt adjacent to penetrators emplaced into volcanic rock at Amboy, California, April 1976, NASA Technical Paper 1026, pp. 1–15.
- Blanchard, M., Bunch, T., Davis, A., Kyte, F., Shade, H., Erlichman, J., Polkowski, G., 1977b. Results of analyses performed on soil adjacent to penetrators emplaced into sediments at McCook, Nebraska, January 1977, NASA Technical Note D-8500, pp. 1–28.
- Carlsaw, H.S., Jaeger, J.C., 2000. *Conduction of Heat in Solids*. Oxford University Press, Oxford.
- Fasso, L., Chao, B.T., Soo, S.L., 1982. Measurement of electrostatic charges and concentration of particles in the freeboard of a fluidized bed. *Powder Technol.* 33, 211–221.
- Ferguson, D.C., Kolecki, J.C., Siebert, M., Wilt, D.M., Matijevic, J.R., 1999. Evidence for Martian electrostatic charging and abrasive wheel wear from the wheel abrasion experiment on the Pathfinder Sojourner Rover. *J. Geophys. Res.* 104, 8747–8789.
- French, A.P., 1957. Penetration of Ballistic Projectiles, Technical Note 10-57-P3, University of South Carolina Department of Physics.
- Hakala, W.W., 1965. Summary of resistance of a granular medium to normal impact of a rigid projectile. Ph.D. thesis, Civil Engineering, Virginia Polytechnic Institute.
- Hendrick, J.G., Gill, W.R., 1977. A critical soil deformation velocity? Conference on Rapid Penetration of Terrestrial Materials, Texas A&M University, pp. 243–250.
- Jayaraj, E.R., 1991. Charge separation during the impact of sand on ice and its relevance to theories of thunderstorm electrification. *Atmos. Res.* 26, 407–424.
- Johnson, J.B., 2001. A Micromechanical theory of penetration, In: Kömle, N. et al. (Eds.), Proceedings, International Workshop on Penetrometry in the Solar System, Graz, Austria October 1999, Austrian Academy of Sciences, Vienna.
- Kargl, G., Macher, W., Kömle, N., Thiel, M., Rohe, C., Ball, A.J., 2001. Accelerometry measurements using the Rosetta Lander's anchoring harpoon: experimental set-up, data reduction and signal analysis. *Planet. Space Sci.* 49, 425–435.
- Kochan, H., Feibig, W., Konopka, U., Kretschmer, M., Mölmann, D., Seidensticker, K.J., Arnold, W., Gebhardt, W., Licht, R., 2000. CASSE—The Rosetta Lander Comet Acoustic Surface Sounding Experiment—status of some aspects, the technical realisation and laboratory simulations. *Planet. Space Sci.* 48, 385–399.
- Kömle, N.I., Ball, A.J., Kargl, G., Stocker, J., Thiel, M., Jolly, H.S., Dziruni, M., Zarnecki, J.C., 1997. Using the anchoring device of a comet lander to determine surface mechanical properties. *Planet. Space Sci.* 45 (12), 1515–1538.
- Kömle, N., Ball, A.J., Kargl, G., Keller, T., Macher, W., Thiel, M., Stöcker, J., Rohe, C., 2001. Impact penetrometry on a comet nucleus—interpretation of laboratory data using penetration models. *Planet. Space Sci.* 49, 575–598.
- Kumano, A., Goldsmith, W., 1982. Projectile impact on soft, porous rock. *Rock Mechan.* 15, 113.
- Lorenz, R.D., Moersch, J.E., Stone, J.A., Morgan Jr., A.R., Smrekar, S.E., 2000. Penetration tests on the DS-2 Mars microprobes: penetration depth and impact accelerometry. *Planet. Space Sci.* 48 (2000), 419–436.
- Lorenz, R.D., Shandera, S.E., 2000. Penetrator launch diagnostics from breech pressure measurements during operation of an air cannon. *Meas. Sci. Technol.* 11, 1819–1823.
- Lorenz, R.D., Ball, A.J., 2001. Review of penetration tests and theories. In: Kömle N, et al. (Eds.), Proceedings, International Workshop on Penetrometry in the Solar System, Graz, Austria, October 1999, Austrian Academy of Sciences, Vienna.
- Lundgren, R., 1995. Personal Communication.
- Pitts, W., Canning, T.N., 1976. Influence of penetrator on local soil temperatures. Appendix K, NASA TM X-73,181 (Blanchard et al., 1976a), pp. 208–217.
- Reece, E., 1976. Penetration test into instrumented target. Appendix L, NASA TM X-73,181 (Blanchard et al., 1976a) pp. 218–220.
- Schmidt, D.S., Schmidt, R.A., Dent, J.D., 1998. Electrostatic force on saltating sand. *J. Geophys. Res.* 103 (D8), 8997–9001.
- Seiferlin, K., Kömle, N., Kargl, G., Spohn, T., 1996. Line Heat Source measurements of the thermal conductivity of porous H₂O ice, CO₂ ice and mineral powders under space conditions. *Planet. Space Sci.* 44, 691–704.
- Serridge, M., Licht, T.R., 1987. *Piezoelectric Accelerometer and Vibration Preamplifier Handbook*, Brüel and Kjaer, Naerum, Denmark.
- Smrekar, S.E., Catling, D., Lorenz, R.D., Magalhaes, J., Meyer, M., Moersch, J., Morgan, P., Murphy, J., Murray, B., Presley-Holloway, M., Yen, A., Zent, A., 1999. The DS-2 Mars Microprobe Mission. *J. Geophys. Res.* 104 (E11), 27,013–27,030.
- Smrekar, S.E., Lorenz, R.D., Urquhart, M., 2001. The Deep Space 2 design and its use for accelerometry and estimation of thermal conductivity. In: Kömle N, et al. (Eds.), Proceedings, International Workshop on Penetrometry in the Solar System, Graz, Austria, October 1999, Austrian Academy of Sciences, Vienna.
- Surkov, Yu.A., Moskaleva, L.P., Shcheglov, O.P., Sheretov, E.P., Kremnev, R.S., Pichkhadze, K.M., Akulov, Yu.P., Dolgoplov, V.P., 1999. Lander and scientific equipment for exploring of volatiles on the Moon. *Planet. and Space Sci.* 47, 1051–1060.
- Yashima, S., Kanda, Y., Sano, S., 1987. Relationships between particle size and fracture energy or impact velocity required to fracture as estimated from single particle crushing. *Powder Technol.* 51, 277–282.